

SAE 4620 Carburized Case Steel Iteration #54

MICROSTRUCTURAL DATA, MONOTONIC AND FATIGUE TEST RESULTS

F. Yin and A. Fatemi

Department of Mechanical, Industrial, and
Manufacturing Engineering
The University of Toledo
Toledo, OH 43606

Prepared for:

The AISI Bar Steel Applications Group

August 2002



**American
Iron and Steel
Institute**

American Iron and Steel Institute
2000 Town Center, Suite 320
Southfield, Michigan 48075
tel: 248-945-4777
fax: 248-352-1740
www.autosteel.org

TABLE OF CONTENTS

SUMMARY	1
I. EXPERIMENTAL PROGRAM	2
1.1 MATERIAL AND SPECIMEN FABRICATION.....	2
1.1.1 Material	2
1.1.2 Specimen.....	2
1.2 TESTING EQUIPMENT.....	3
1.2.1 Apparatus.....	3
1.2.2 Alignment.....	4
1.3 TEST METHODS AND PROCEDURES	5
1.3.1 Monotonic tension tests	5
1.3.2 Constant amplitude fatigue tests.....	6
II. EXPERIMENTAL RESULTS AND ANALYSIS.....	7
2.1 MICROSTRUCTURAL DATA.....	7
2.2 MONOTONIC DEFORMATION BEHAVIOR.....	8
2.3 CYCLIC DEFORMATION BEHAVIOR.....	10
2.3.1 Transient cyclic deformation.....	10
2.3.2 Steady-state cyclic deformation.....	10
2.4 CONSTANT AMPLITUDE FATIGUE BEHAVIOR	12
REFERENCES.....	27
APPENDIX.....	28

NOMENCLATURE

A_o, A_f	initial, final area	S	engineering stress
HB, HRB, HRC	Brinell, Rockwell B-Scale, Rockwell C-Scale hardness number	YS, UYS, LYS, YS'	monotonic yield, upper yield, lower yield, cyclic yield strength
b, c, n	fatigue strength, fatigue ductility, strain hardening exponent	YPE	yield point elongation
D_o, D_f	initial, final diameter	S_u	ultimate tensile strength
e	engineering strain	%EL	percent elongation
E, E'	monotonic, midlife cycle modulus of elasticity	%RA	percent reduction in area
K, K'	monotonic, cyclic strength coefficient	$\sigma, \sigma_f, \sigma_f'$	true stress, true fracture strength, fatigue strength coefficient
L_o, L_f	initial, final gage length	$\sigma_a, \sigma_m, \Delta\sigma$	stress amplitude, mean stress, stress range
$N_{50\%}, (N_f)_{10\%},$ $(N_f)_{50\%},$	number of cycles to midlife, 10% load drop, 50% load drop	$\epsilon_e, \epsilon_p, \epsilon$	true elastic, plastic, total strain
$2N_f$	reversals to failure	ϵ_f, ϵ_f'	true fracture ductility, fatigue ductility coefficient
P_f, P_u	fracture, ultimate load	$\epsilon_a, \epsilon_m, \Delta\epsilon$	strain amplitude, mean strain, strain range
R	neck radius; or strain ratio	$\Delta\epsilon_e, \Delta\epsilon_p$	elastic, plastic strain range

UNIT CONVERSION TABLE

<u>Measure</u>	<u>SI Unit</u>	<u>US Unit</u>	<u>from SI to US</u>	<u>from US to SI</u>
Length	mm	in	1 mm = 0.03937 in	1 in = 25.4 mm
Area	mm ²	in ²	1 mm ² = 0.00155 in ²	1 in ² = 645.16 mm ²
Load	kN	klb	1kN = 0.2248 klb	1 klb = 4.448 kN
Stress	MPa	ksi	1 MPa = 0.14503 ksi	1 ksi = 6.895 MPa
Temperature	°C	°F	°C = (°F - 32)/1.8	°F = (°C * 1.8) + 32

<u>In SI Unit:</u>	1 kN = 10 ³ N	1 Pa = 1 N/m ²	1 MPa = 10 ⁶ Pa = 1 N/mm ²	1 Gpa = 10 ⁹ Pa
<u>In US Unit:</u>	1 klb = 10 ³ lb	1 psi = 1 lb/in ²	1 ksi = 10 ³ psi	

SUMMARY

The monotonic properties, and fatigue behavior data have been obtained for SAE 4620 Carburized Case steel. The material was provided by MacSteel Company. Two tensile tests were performed to acquire the desired monotonic properties. Eighteen fatigue tests were performed to obtain the strain-life and cyclic stress-strain curves and properties. The experimental procedure followed and results obtained are presented and discussed in this report.

I. EXPERIMENTAL PROGRAM

1.1 Material and Specimen Fabrication

1.1.1 Material

The SAE 4620 Carburized Case steel was provided by MacSteel Company. This material was delivered to the University of Toledo in round bar form. The bars were approximately 1.875 inch in diameter. They were reduced to bars approximately 0.5 inch diameter by EDM, then heat treated and ground after machining. In Table 1, the chemical composition supplied by AISI is shown.

1.1.2 Specimen

In this study, identical round specimens were used for the monotonic and fatigue tests. The specimen configuration and dimensions are shown in Figure 1. This configuration deviates slightly from the specimens recommended by ASTM Standard E606 [1]. The recommended specimens have uniform or hourglass test sections. The specimen geometry shown in Figure 1 differs by using a large secondary radius throughout the test section.

All specimens were machined in the Mechanical, Industrial, and Manufacturing Engineering Machine Shop at the University of Toledo. The specimens were initially turned on a lathe to an appropriate diameter for insertion into a CNC machine. Using the CNC machine, final turning was performed to achieve the tolerable dimensions specified on the specimen drawings.

A commercial round-specimen polishing machine was used to polish the specimen gage section. Four different grits of aluminum oxide lapping film were used: 30 μ , 15 μ , 9 μ , and 3 μ .

The 3 μ grit was used as the final polish and polishing marks coincided with the specimens' longitudinal direction. The polished surfaces were carefully examined under magnification to ensure complete removal of machine marks within the test section.

1.2 Testing Equipment

1.2.1 Apparatus

An MTS closed-loop servo-controlled hydraulic axial load frame in conjunction with a Schenck-Pegasus digital servo-controller was used to conduct the tests. The calibration of this system was verified prior to beginning the test program. The load cell used had a capacity of 22 klb. Hydraulically operated grips using universal tapered collets were employed to secure the specimens' ends in series with the load cell.

Total strain was controlled for all tests using an extensometer rated as ASTM class B1 [2]. The calibration of the extensometer was verified using displacement apparatus containing a micrometer barrel in divisions of 0.0001 in. The extensometer had a gage length of 0.30 in and was capable of measuring strains up to 15 %.

In order to protect the specimens' surface from the knife-edges of the extensometer, ASTM Standard E606 recommends the use of transparent tape or epoxy to 'cushion' the attachment. For this study, it was found that application of transparent tape strips was difficult due to the radius within the test section. Therefore, epoxy was considered to be the best protection. One disadvantage of epoxy is the variability of mixtures throughout the test program. As an alternative to epoxy, M-coat D offered a more consistent mixture. Therefore, the tests were

performed using M-coat D.

All tests were conducted at room temperature and were monitored using a digital thermometer. In order to minimize temperature effects upon the extensometer and load cell calibrations, fluctuations were maintained within ± 2 °C (± 3.6 °F) as required by ASTM Standard E606. Also, the relative humidity of the air was monitored using a precision hydrometer.

1.2.2 Alignment

Significant effort was put forth to align the load train (load cell, grips, specimen, and actuator). Misalignment can result from both tilt and offset between the central lines of the load train components. According to ASTM Standard E606, the maximum bending strains should not exceed 5 % of the minimum axial strain range imposed during any test program. For this study, the minimum axial strain range was 0.0065 in/in. Therefore, the maximum allowable bending strain was 325 microstrain. ASTM Standard E1012, Type A, Method 1 was followed to verify specimen alignment [3]. For this procedure, two arrays of four strain gages per array were arranged at the upper and lower ends of the uniform gage section. For each array, gages were equally spaced around the circumference of a 0.5-in. uniform diameter bar. The maximum bending strain determined from the gaged specimen was less than 60 microstrain. This value was well within the allowable ASTM limit.

1.3 Test Methods and Procedures

1.3.1 Monotonic tension tests

All monotonic tests in this study were performed using test methods specified by ASTM Standard E8 [4]. Two specimens were used to obtain the monotonic properties. Strain control was used until fracture.

For the elastic and initial yield region (0% to 0.5% strain), a strain rate of 0.0025 in/in/min was chosen. This strain rate was three-quarters of the maximum allowable rate specified by ASTM Standard E8 for the initial yield region. After yielding (0.5% strain to fracture), the strain rate was increased by a factor of three (i.e., 0.0075 in/in/min).

After the tension tests were concluded, the broken specimens were carefully reassembled. The final gage lengths of the fractured specimens were measured with a Vernier caliper having divisions of 0.001 in. Using an optical comparator with 10X magnification and divisions of 0.001 in, the final diameter and the neck radius were measured. It should be noted that prior to the test, the initial minimum diameter was measured with this same instrument.

1.3.2 Constant amplitude fatigue tests

All constant amplitude fatigue tests in this study were performed according to ASTM Standard E606. It is recommended by this standard that at least 10 specimens be used to generate the fatigue properties. For this study, 18 specimens at 7 different strain amplitudes ranging from 0.325% to 1.225% were utilized. LabVIEW by National Instrument was used to record the hysteresis loops.

There were two control modes used for these tests. Strain control was initially used in the tests with plastic deformation (1.225%, 1.1%, 0.9% and 0.7% strain amplitude), after certain cycles load control was used for the remainder of the test. For the all elastic tests (0.5%, 0.4% and 0.325% strain amplitude), load control was used all through the tests. For the tests starting with strain control, the applied frequencies ranged from 0.1 Hz to 0.5 Hz in order to keep a strain rate about 0.02 in/in/sec. For the load control tests, the frequency was increased between 2 Hz and 30 Hz in order to shorten the overall test duration. All strain control tests were conducted using a triangular waveform.

II. EXPERIMENTAL RESULTS AND ANALYSIS

2.1 Microstructural Data

Photomicrographs of the microstructure were obtained using an optical microscope with a digital camera attachment. In Figure 2, the longitudinal direction is shown at 500X magnification. It can be seen from this photomicrograph that SAE 4620 Carburized Case steel had a martensite microstructure. In Figure 3a, the inclusions/voids in L-T direction are shown at 100X magnification. For Figures 2 and 3a, the rolling direction is horizontal to the page. The subsurface crack in one of the broken specimens is shown in Figure 3b at 50X magnification. The subsurface crack initiating from the inclusion in the specimen is shown in Figure 3c at 100X magnification.

According to ASTM Standard E45, method A, the inclusion rating number for type A inclusion in L-T direction was found [6]. Rockwell hardness tests were also performed. A summary of the microstructural data for SAE 4620 Carburized Case steel is provided in Table 2.

2.2 Monotonic Deformation Behavior

The properties determined from monotonic tests were the following: modulus of elasticity (E), yield strength (YS), ultimate tensile strength (S_u), percent elongation (%EL), percent reduction in area (%RA), true fracture strength (σ_f), true fracture ductility (ϵ_f), strength coefficient (K), and strain hardening exponent (n).

True stress (σ), true strain (ϵ), and true plastic strain (ϵ_p) were calculated from engineering stress (S) and engineering strain (e), according to the following relationships which are based on constant volume assumption:

$$\sigma = S(1 + e) \quad (1a)$$

$$\epsilon = \ln(1 + e) \quad (1b)$$

$$\epsilon_p = \epsilon - \epsilon_e = \epsilon - \frac{\sigma}{E} \quad (1c)$$

The true stress (σ) - true strain (ϵ) plot is often represented by the Ramberg-Osgood equation:

$$\epsilon = \epsilon_e + \epsilon_p = \frac{\sigma}{E} + \left(\frac{\sigma}{K} \right)^{\frac{1}{n}} \quad (2)$$

The strength coefficient, K, and strain hardening exponent, n, are the intercept and slope of the best line fit to true stress (σ) versus true plastic strain (ϵ_p) data in log-log scale:

$$\sigma = K \left(\epsilon_p \right)^n \quad (3)$$

In accordance with ASTM Standard E739 [8], when performing the least squares fit, the true plastic strain (ϵ_p) was the independent variable and the stress (σ) was the dependent variable. These plots for the two tests conducted are shown in Figure 4. To generate the K and n values, the range of data used in this figure was chosen according to the definition of discontinuous yielding specified in ASTM Standard E646 [9]. Therefore, the valid data range occurred between the end of yield point extension and the strain at or prior to maximum load.

The true fracture strength, σ_f , was corrected for necking according to the Bridgman correction factor [9]:

$$\sigma_f = \frac{\frac{P_f}{A_f}}{\left(1 + \frac{4R}{D_f}\right) \ln\left(1 + \frac{D_f}{4R}\right)} \quad (4)$$

where P_f is the load at fracture, R is the neck radius, and D_f is the diameter at fracture.

The true fracture ductility, ϵ_f , was calculated from the relationship based on constant volume:

$$\epsilon_f = \ln\left(\frac{A_o}{A_f}\right) = \ln\left(\frac{1}{1 - RA}\right) \quad (5)$$

where A_f is the cross-sectional area at fracture, A_o is the original cross-sectional area, and RA is the reduction in area.

A summary of the monotonic properties for SAE 4620 Carburized Case steel is provided in Table 2. The monotonic stress-strain curves are shown in Figure 5. As can be seen from this figure, the two curves are very close to each other. Refer to Table A.1 in the Appendix for a summary of the monotonic test results.

2.3 Cyclic Deformation Behavior

2.3.1 Transient cyclic response

Transient cyclic response describes the process of cyclic-induced change in deformation resistance of a material. Data obtained from constant amplitude strain-controlled fatigue tests were used to determine this response. Plots of stress amplitude variation versus applied number of cycles can indicate the degree of transient cyclic softening/hardening. Also, these plots show when cyclic stabilization occurs. A composite plot of the transient cyclic response for SAE 4620 Carburized Case steel is shown in Figure A.1 of the Appendix. The transient response was normalized on the rectangular plot in Figure A.1a, while a semi-log plot is shown in Figure A.1b. Even though multiple tests were conducted at each strain amplitude, data from one test at each strain amplitude tested are shown in these plots.

2.3.2 Steady-state cyclic deformation

Another cyclic behavior of interest was the steady state or stable response. Data obtained from constant amplitude strain-controlled fatigue tests were also used to determine this response. The properties determined from the steady-state hysteresis loops were the following: cyclic modulus of elasticity (E'), cyclic strength coefficient (K'), cyclic strain hardening exponent (n'), and cyclic yield strength (YS'). Half-life (midlife) hysteresis loops and data were used to obtain the stable cyclic properties.

Similar to monotonic behavior, the cyclic true stress-strain behavior can be characterized by the Ramberg-Osgood type equation:

$$\frac{\Delta \varepsilon}{2} = \frac{\Delta \varepsilon_e}{2} + \frac{\Delta \varepsilon_p}{2} = \frac{\Delta \sigma}{2 E} + \left(\frac{\Delta \sigma}{2 K'} \right)^{\frac{1}{n'}} \quad (6)$$

It should be noted that in Equation 6 and the other equations that follow, E is the average modulus of elasticity that was calculated from the monotonic tests.

The cyclic strength coefficient, K', and cyclic strain hardening exponent, n', are the intercept and slope of the best line fit to true stress amplitude ($\Delta\sigma/2$) versus true plastic strain amplitude ($\Delta\varepsilon_p/2$) data in log-log scale:

$$\frac{\Delta \sigma}{2} = K' \left(\frac{\Delta \varepsilon_p}{2} \right)^{n'} \quad (7)$$

In accordance with ASTM Standard E739, when performing the least squares fit, the true plastic strain amplitude ($\Delta\varepsilon_p/2$) was the independent variable and the stress amplitude ($\Delta\sigma/2$) was the dependent variable. The true plastic strain amplitude was calculated by the following equation:

$$\frac{\Delta \varepsilon_p}{2} = \frac{\Delta \varepsilon}{2} - \frac{\Delta \sigma}{2 E} \quad (8)$$

This plot is shown in Figure 6. To generate the K' and n' values, the range of data used in the figure was chosen for $[\Delta\varepsilon_p/2]_{\text{calculated}} \geq 0.00020$ in/in.

The cyclic stress - strain curve reflects the resistance of a material to cyclic deformation and can be vastly different from the monotonic stress - strain curve. The cyclic stress - strain curve is shown in Figure 7. In Figure 8, superimposed plots of monotonic and cyclic curves are shown. As can be seen in Figure 8, SAE 4620 Carburized Case steel cyclically hardens.

Figure A.2 in the Appendix shows a composite plot of the steady-state (midlife) hysteresis loops. Even though multiple tests were conducted at each strain amplitude, the stable loops from only one test at each strain amplitude are shown in this plot.

2.4 Constant Amplitude Fatigue Behavior

Constant amplitude strain-controlled fatigue tests were performed to determine the strain-life curve. The following equation relates the true strain amplitude to the fatigue life:

$$\frac{\Delta \varepsilon}{2} = \frac{\Delta \varepsilon_e}{2} + \frac{\Delta \varepsilon_p}{2} = \frac{\sigma'_f}{E} (2 N_f)^b + \varepsilon'_f (2 N_f)^c \quad (9)$$

where σ'_f is the fatigue strength coefficient, b is the fatigue strength exponent, ε'_f is the fatigue ductility coefficient, c is the fatigue ductility exponent, E is the monotonic modulus of elasticity, and $2N_f$ is the number of reversals to failure (which was defined as a 50% load drop, as recommended by ASTM Standard E606).

The fatigue strength coefficient, σ'_f , and fatigue strength exponent, b , are the intercept and slope of the best line fit to true stress amplitude ($\Delta\sigma/2$) versus reversals to failure ($2N_f$) data in log-log scale:

$$\frac{\Delta \sigma}{2} = \sigma'_f (2 N_f)^b \quad (10)$$

In accordance with ASTM Standard E739, when performing the least squares fit, the stress amplitude ($\Delta\sigma/2$) was the independent variable and the reversals to failure ($2N_f$) was the dependent variable. This plot is shown in Figure 9. To generate the σ'_f and b values, the range of data used in this figure was chosen for $N_f \leq 10^6$ cycles.

The fatigue ductility coefficient, ε_f' , and fatigue ductility exponent, c , are the intercept and slope of the best line fit to calculated true plastic strain amplitude ($\Delta\varepsilon_p/2$) versus reversals to failure ($2N_f$) data in log-log scale:

$$\left(\frac{\Delta\varepsilon_p}{2} \right)_{\text{calculated}} = \varepsilon_f' (2N_f)^c \quad (11)$$

In accordance with ASTM Standard E739, when performing the least squares fit, the calculated true plastic strain amplitude ($\Delta\varepsilon_p/2$) was the independent variable and the reversals to failure ($2N_f$) was the dependent variable. The calculated true plastic strain amplitude was determined from Equation 8. This plot is shown in Figure 10. To generate the ε_f' and c values, the range of data used in this figure was chosen for $[\Delta\varepsilon_p/2]_{\text{calculated}} \geq 0.00020$ in/in.

The true strain amplitude versus reversals to failure plot is shown in Figure 11. This plot displays the strain - life curve (Eqn. 9), the elastic strain portion (Eqn. 10), the plastic strain portion (Eqn. 11), and superimposed fatigue data. A summary of the cyclic properties for SAE 4620 Carburized Case steel is provided in Table 2. Table A.2 in the Appendix provides the summary of the fatigue test results.

Table 1: Chemical composition of SAE 4620 Carburized Case steel

<u>Element</u>	<u>Wt. %</u>
Carbon, C	0.2%
Manganese, Mn	0.67%
Phosphorus, P	0.008%
Sulfur, S	0.030%
Silicon, Si	0.200%
Chromium, Cr	0.19%
Nickel, Ni	1.6%
Molybdenum, Mo	0.24%
Copper, Cu	0.16%
Tin, Sn	0.006%
Aluminum, Al	0.027%

Table 2: Summary of the Mechanical Properties

Microstructural Data	Average				
<u>ASTM grain size number (MAG=1000X):</u>					
The first longitudinal direction (L-T)	4 to 5				
<u>Inclusion rating number (MAG=100X):</u>					
Type A (sulfide type), thin series	2 to 2.5				
Type B (alumina type), thin series	None				
Type C (silicate type), thin series	None				
Type D (globular type), thin series	None				
<u>Hardness:</u>					
Brinell (HB)					
Transverse direction (T-T')	NA				
The first longitudinal direction (L-T)	NA				
Rockwell B-scale (HRB)					
Transverse direction (T-T')	NA				
The first longitudinal direction (L-T)	NA				
Rockwell C-scale (HRC)					
Transverse direction (T-T')	61 at the flat grip section (not ground or polished), 54 at the center of the gage section				
The first longitudinal direction (L-T)	NA				
Microstructure type:					
Transverse direction (T-T')	martensitic				
Monotonic Properties		Average		Range	
Modulus of elasticity, E, GPa (ksi):	210.3	(30,494.4)	210.0 - 210.6	(30,451.0 - 30,537.8)	
Yield strength (0.2% offset), YS, MPa (ksi):	1169.1	(169.6)	1144.2 - 1194.1	(165.9 - 173.2)	
Upper yield strength UYS, MPa (ksi):	NA	NA			
Lower yield strength LYS, MPa (ksi):	NA	NA			
Yield point elongation, YPE (%) :	NA				
Ultimate strength, S _u , MPa (ksi):	1775.6	(257.5)	1736.6 - 1814.5	(251.9 - 263.2)	
Percent elongation, %EL (%) :	7.7%		7.7% - 7.7%		
Percent reduction in area, %RA (%) :	1.4%		0.9% - 1.9%		
Strength coefficient, K, MPa (ksi):	7,717.7	(1,119.3)	6,180.6 - 9,254.8	(896.4 - 1342.2)	
Strain hardening exponent, n:	0.3029		0.2639 - 0.3419		
True fracture strength, σ _f [*] , MPa (ksi):	1788.9	(259.5)	1758.7 - 1819.2	(255.1 - 263.8)	
True fracture ductility, ε _f (%) :	1.4%		0.9% - 2.0%		
Cyclic Properties		Average		Range	
Cyclic modulus of elasticity, E', GPa (ksi):	205.6	(29,825.3)	200.0 - 217.9	(200.0)	(217.9)
Fatigue strength coefficient, σ _f ['] , MPa (ksi):	3,129.3	(453.9)			
Fatigue strength exponent, b:	-0.0996				
Fatigue ductility coefficient, ε _f ['] :	0.0071				
Fatigue ductility exponent, c:	-0.3843				
Cyclic yield strength, YS', MPa (ksi)	2131.5	(309.1)			
Cyclic strength coefficient, K', MPa (ksi):	7,344.4	(1,065.2)			
Cyclic strain hardening exponent, n':	0.1991				

*Correction was made according to Bridgman correction factor.

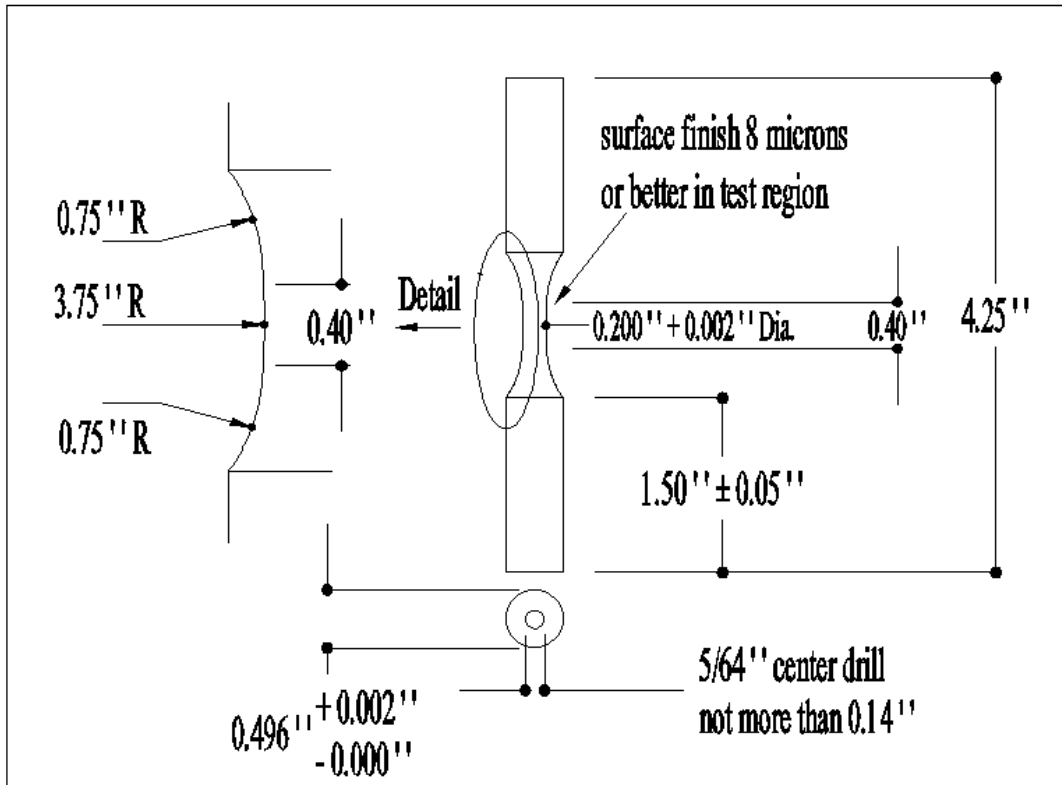


Figure 1: Specimen configuration and dimensions



Figure 2: Photomicrograph in transverse direction (T-T') at 500X for SAE 4620 Carburized Case steel (rolling direction is horizontal)



Figure 3a: Examples of inclusions in the transverse direction (T-T') at 100X for SAE 4620 Carburized Case steel (rolling direction is horizontal)



Figure 3b: Subsurface crack at 50X for SAE 4620 Carburized steel



Figure 3c: Subsurface crack at 100X for SAE 4620 Carburized steel

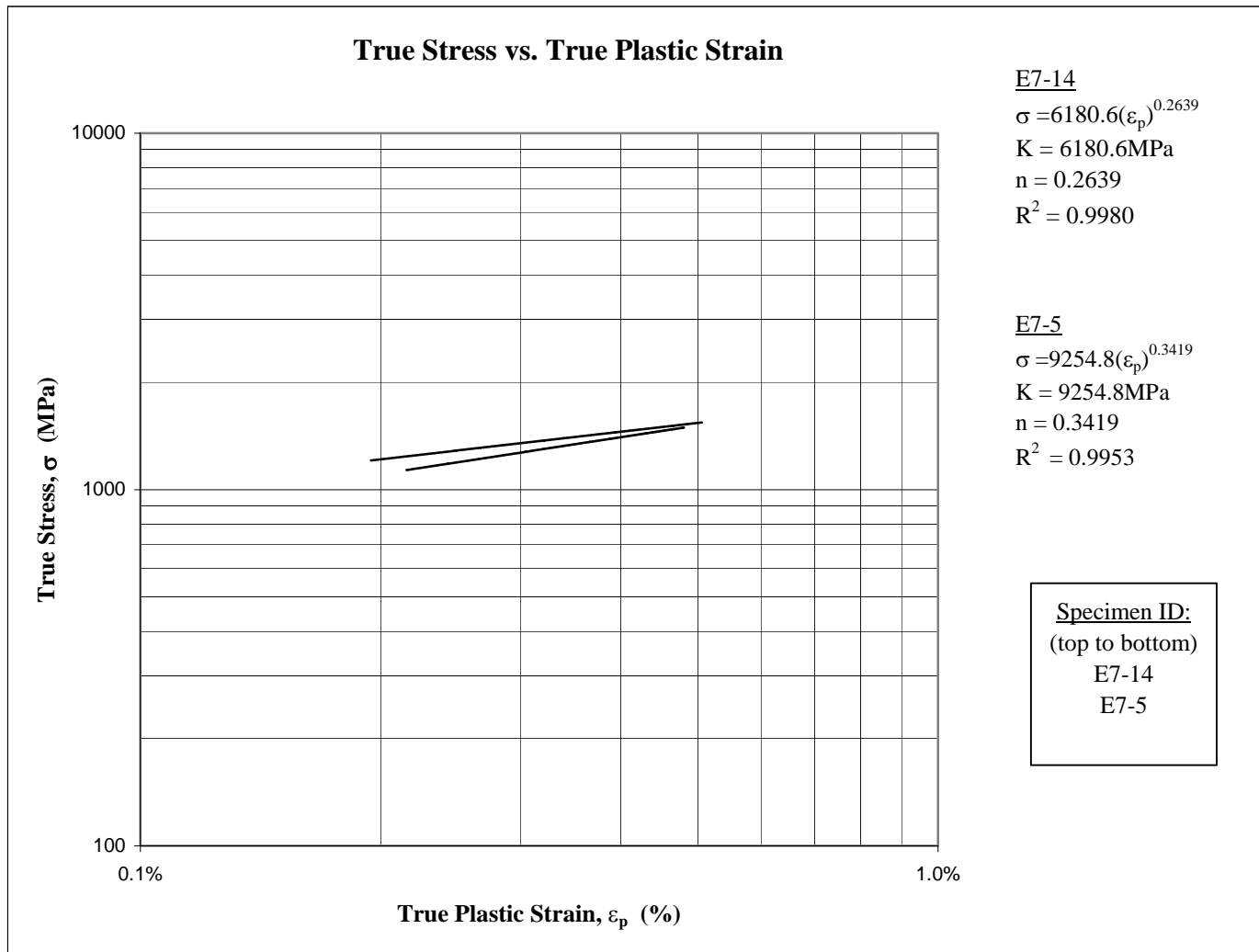


Figure 4: True stress versus true plastic strain

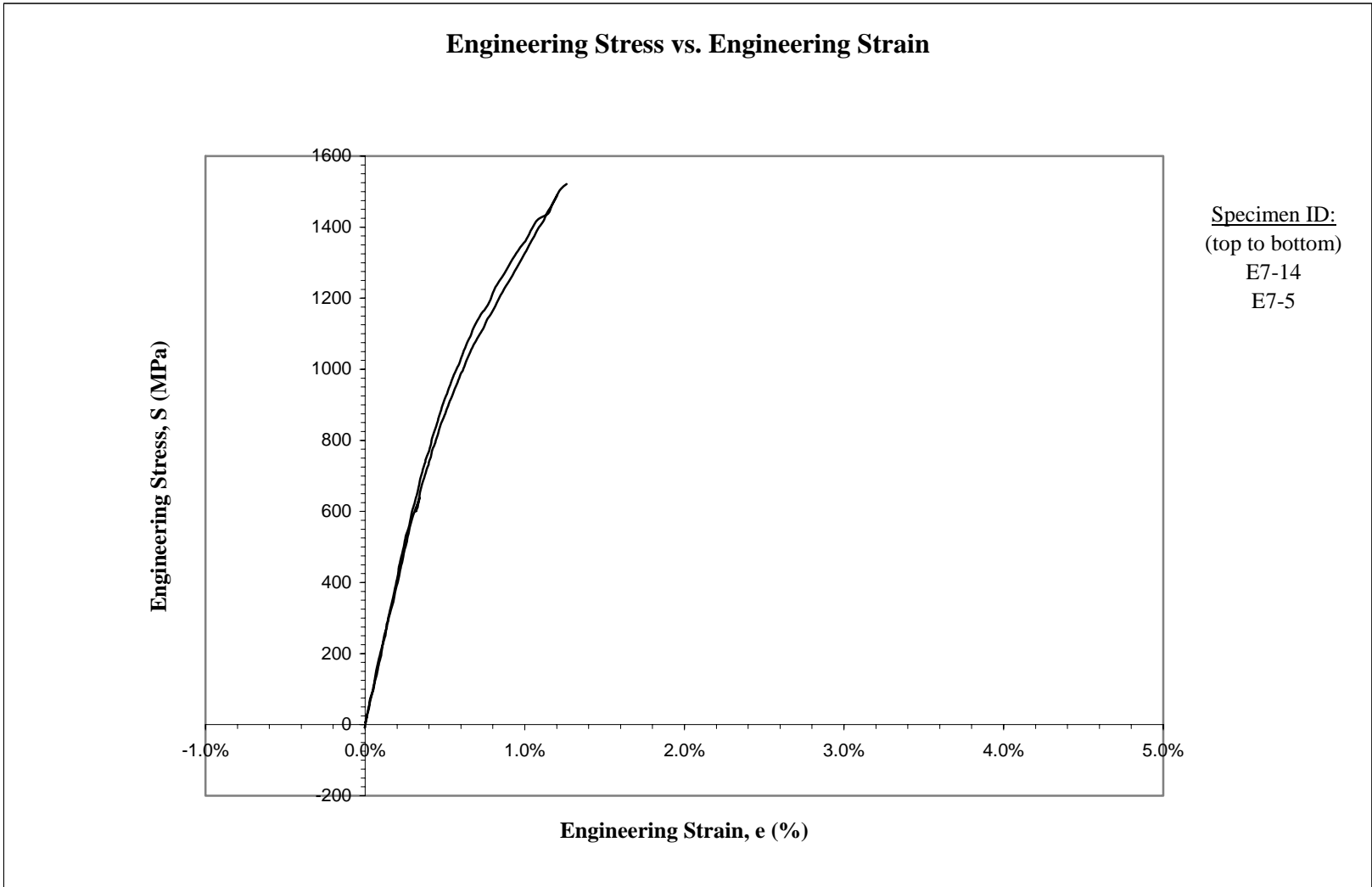


Figure 5: Monotonic stress-strain curve

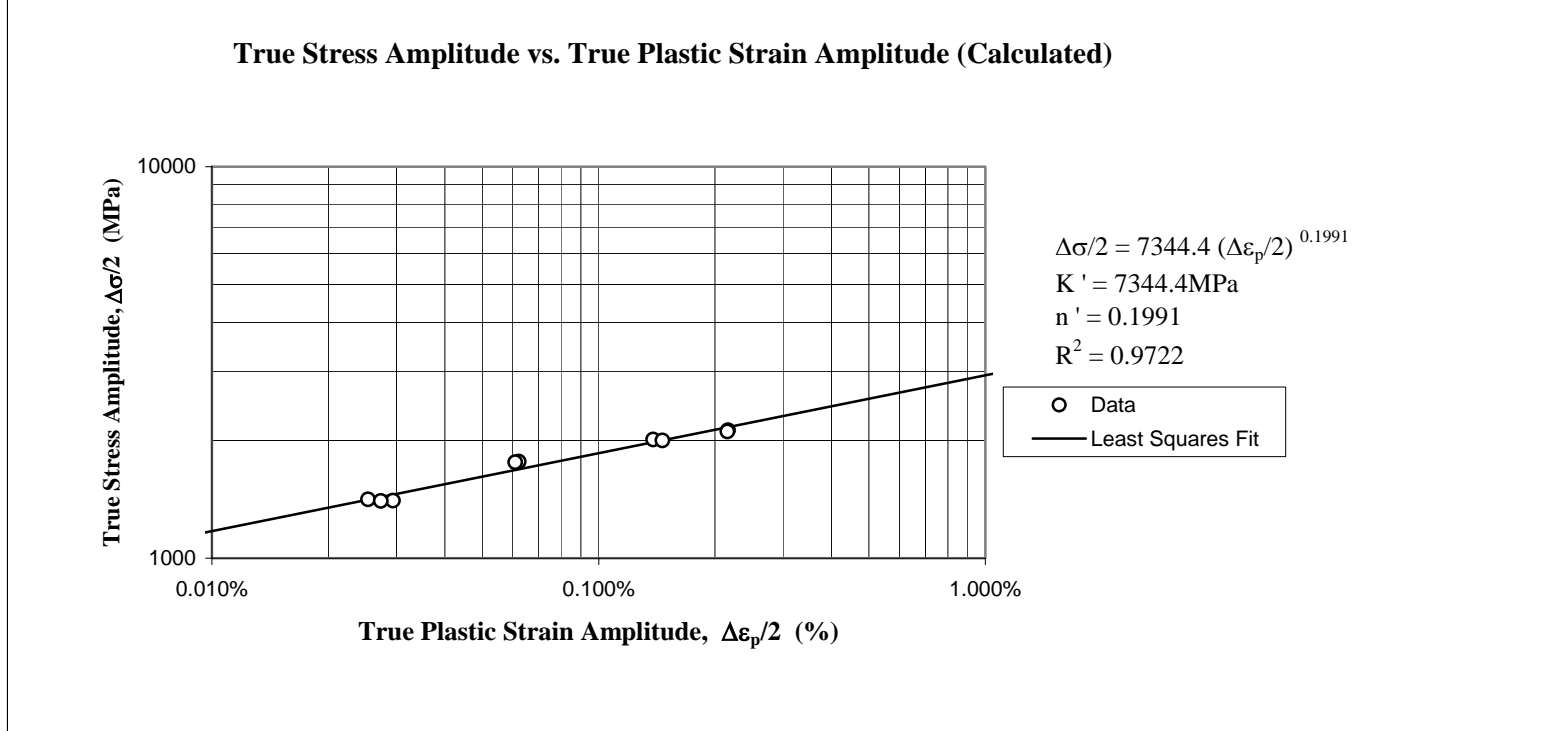


Figure 6: True stress amplitude versus calculated true plastic strain amplitude

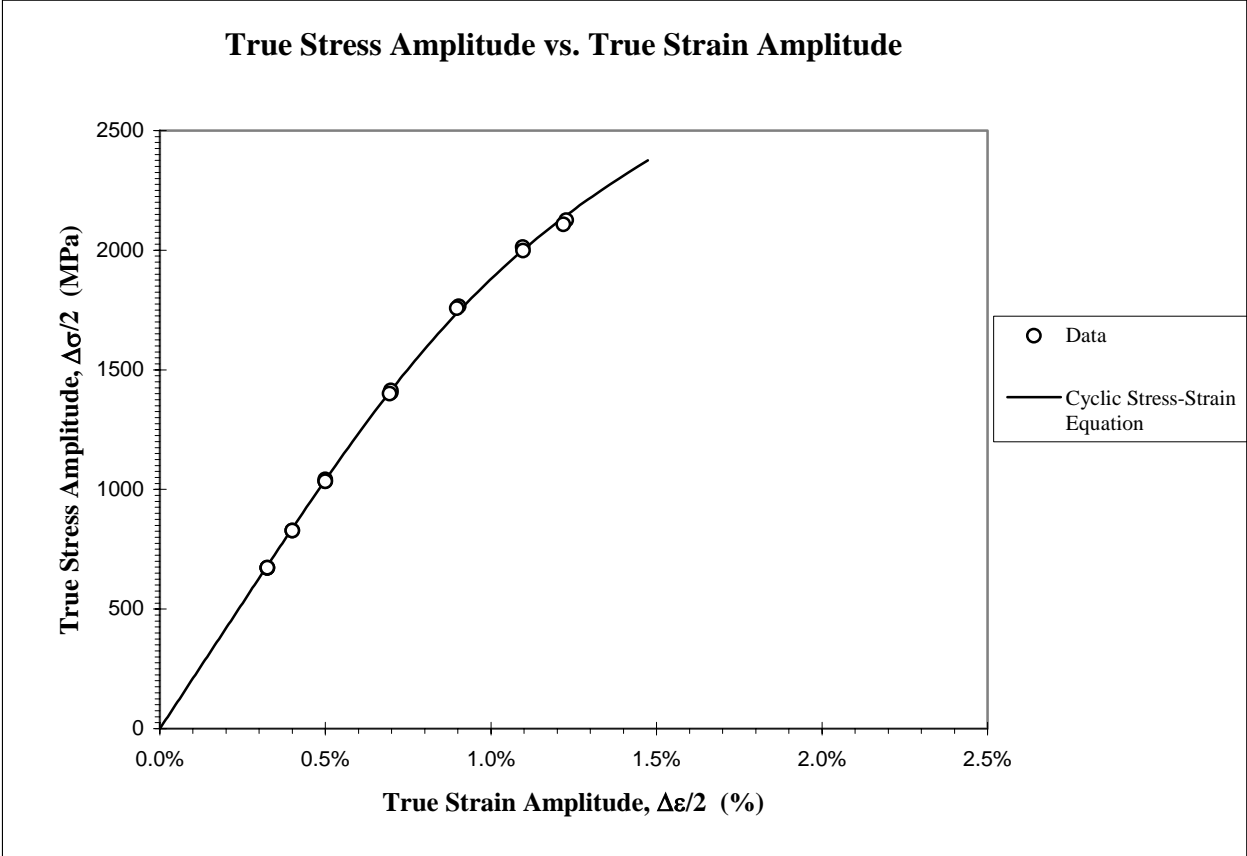


Figure 7: True stress amplitude versus true strain amplitude

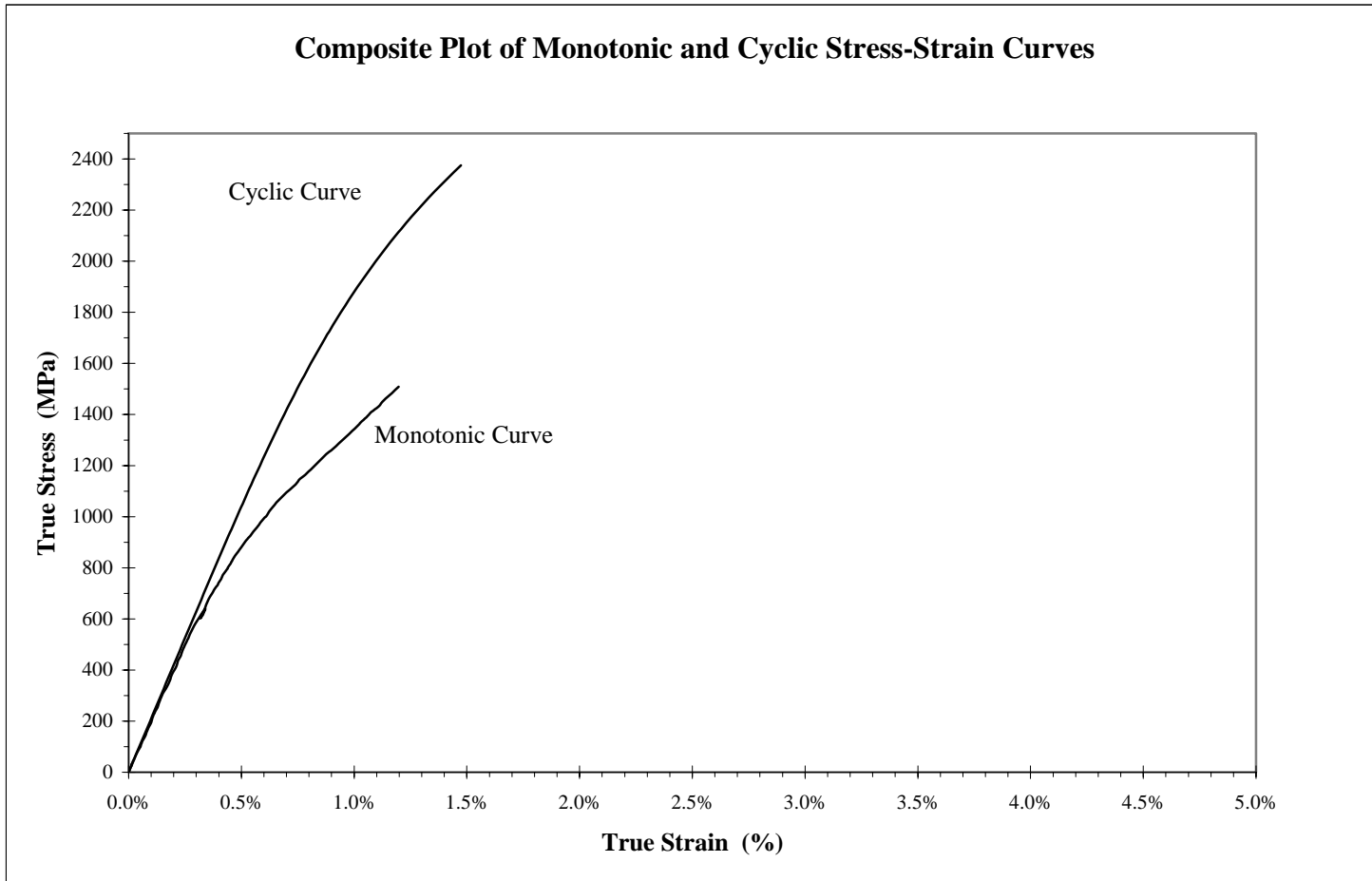


Figure 8: Composite plot of cyclic and monotonic stress-strain curves

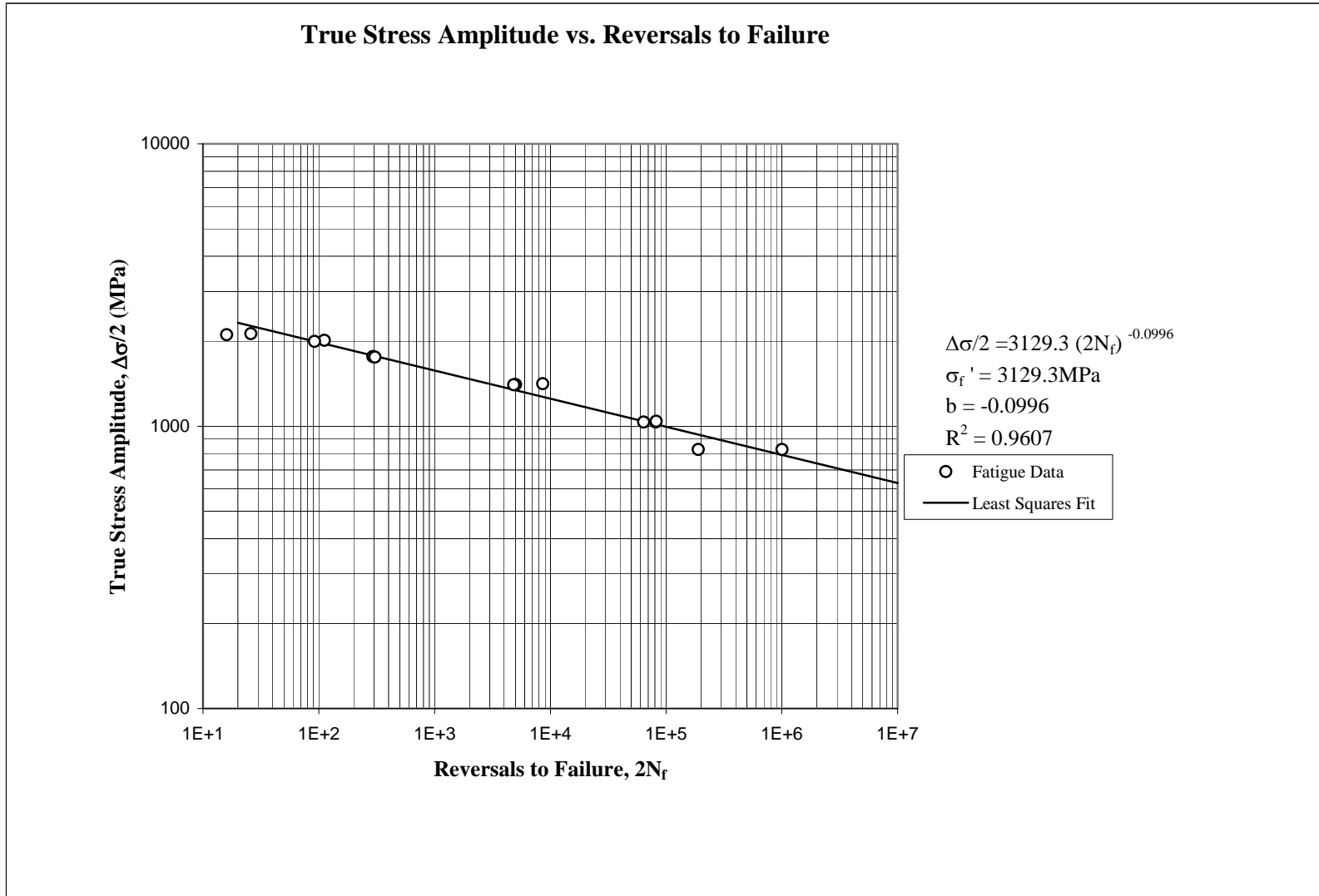


Figure 9: True stress amplitude versus reversals to failure

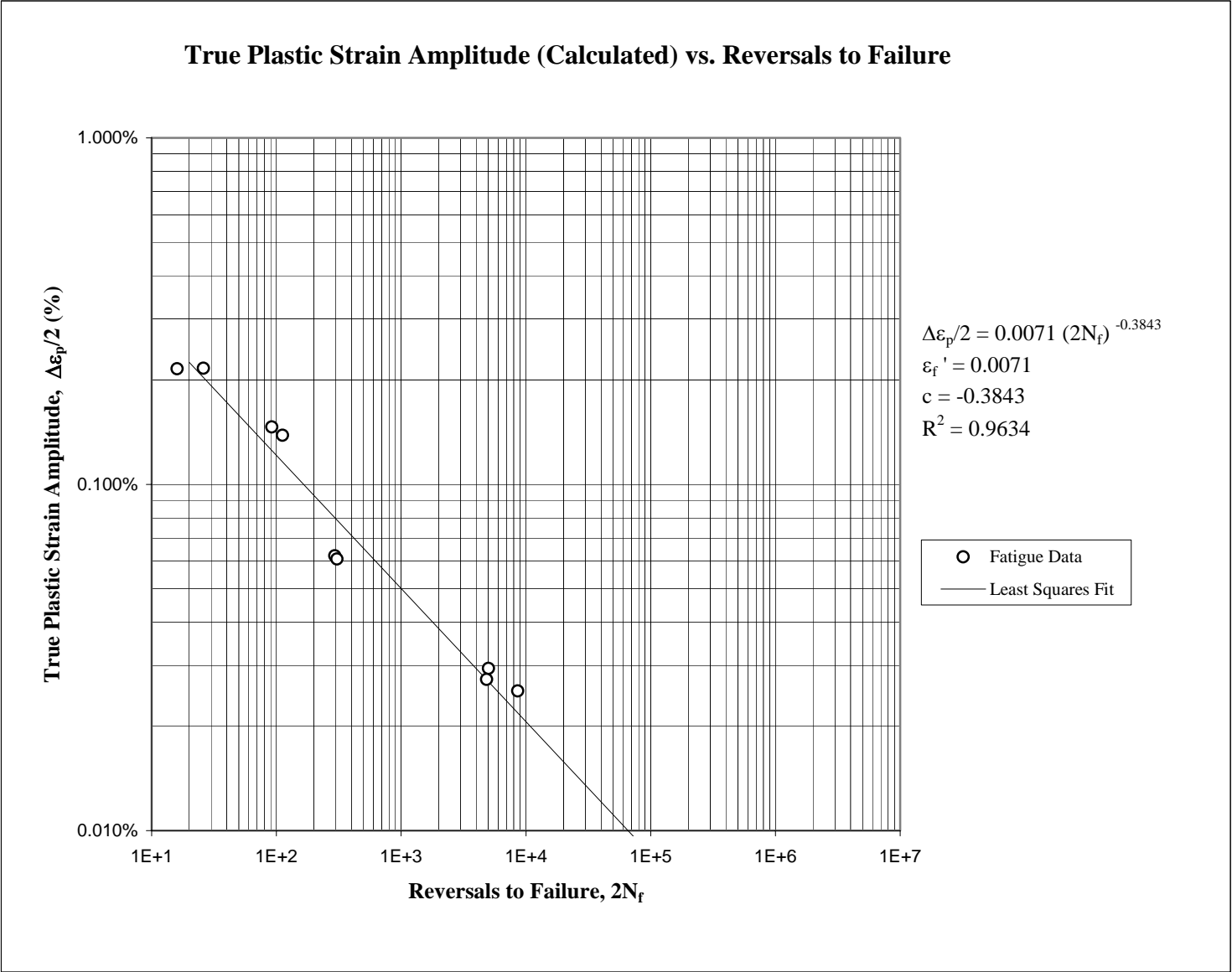


Figure 10: Calculated true plastic strain amplitude versus reversals to failure

True Strain Amplitude vs. Reversals to Failure

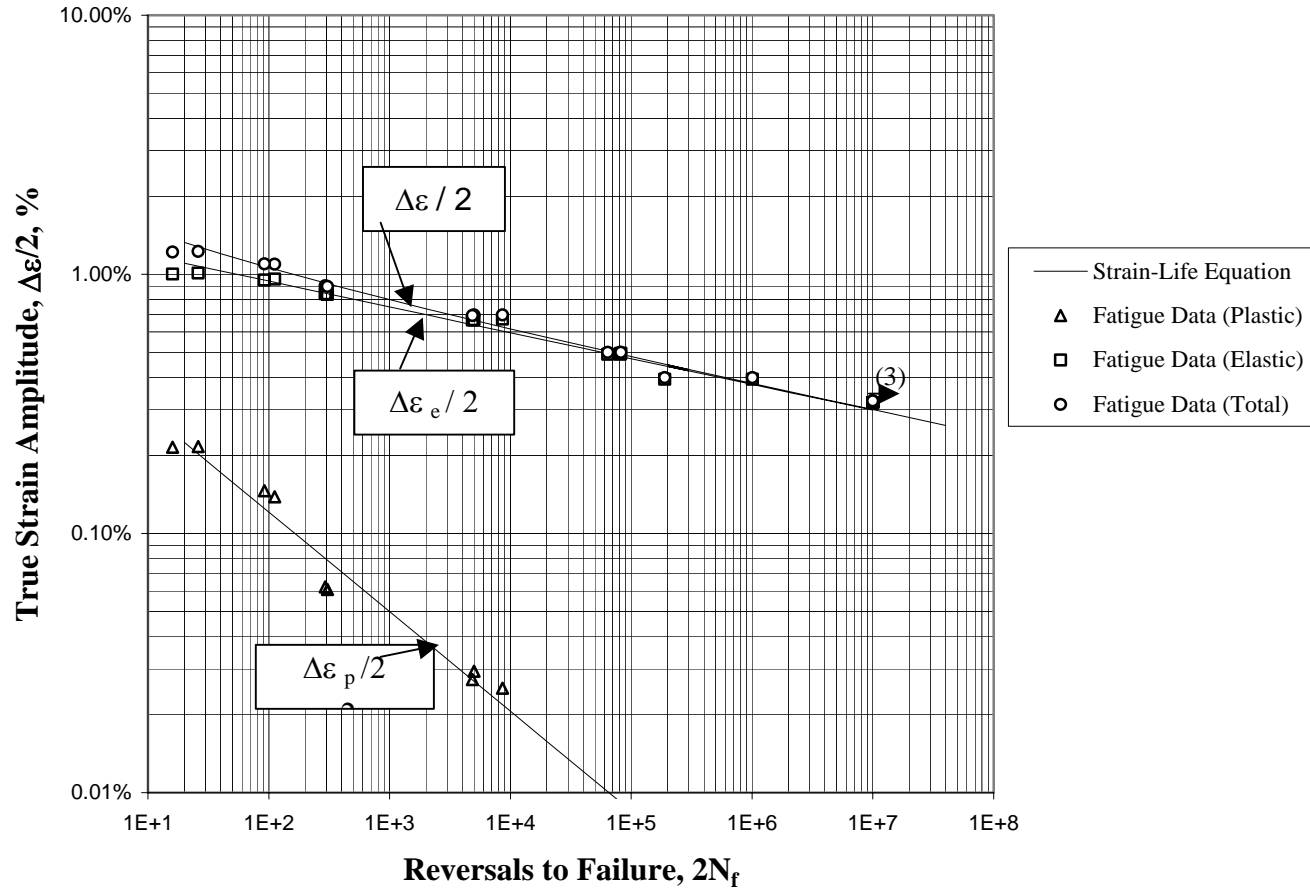


Figure 11: True strain amplitude versus reversals to failure

REFERENCES

- [1] ASTM Standard E606-92, "Standard Practice for Strain-Controlled Fatigue Testing," Annual Book of ASTM Standards, Vol. 03.01, 1997, pp. 523-537.
- [2] ASTM Standard E83-96, "Standard Practice for Verification and Classification of Extensometers," Annual Book of ASTM Standards, Vol. 03.01, 1997, pp. 198-206.
- [3] ASTM Standard E1012-93a, "Standard Practice for Verification of Specimen Alignment Under Tensile Loading," Annual Book of ASTM Standards, Vol. 03.01, 1997, pp. 699-706.
- [4] ASTM Standard E8-96a, "Standard Test Methods for Tension Testing of Metallic Materials," Annual Book of ASTM Standards, Vol. 03.01, 1997, pp. 56-76..
- [5] ASTM Standard E112-96, "Standard Test Methods for Determining Average Grain Size," Annual Book of ASTM Standards, Vol. 03.01, 1997, pp. 227-249.
- [6] ASTM Standard E45-97, "Standard Test Methods for Determining the Inclusion Content of Steel," Annual Book of ASTM Standards, Vol. 03.01, 1997, pp. 157-170.
- [7] ASTM Standard E739-91, "Standard Practice for Statistical Analysis of Linear or Linearized Stress-Life (S-N) and Strain-Life (ϵ -N) Fatigue Data," Annual Book of ASTM Standards, Vol. 03.01, 1995, pp. 615-621.
- [8] ASTM Standard E646-93, "Standard Test Method for Tensile Strain-Hardening Exponents (n-values) of Metallic Sheet Materials," Annual Book of ASTM Standards, Vol. 03.01, 1997, pp. 550-556.
- [9] Bridgman, P. W., "Stress Distribution at the Neck of Tension Specimen," *Transactions of American Society for Metals*, Vol. 32, 1944, pp. 553-572.

APPENDIX

Table A.1: Summary of monotonic tensile test results

Specimen ID	D _o , mm (in.)	D _f , mm (in.)	L _o , mm (in.)	L _f , mm (in.)	E, GPa (ksi)	YS (offset=0.2%), MPa (ksi)	UYS, MPa (ksi)	LYS, MPa (ksi)	YPE , %	S _u , MPa (ksi)	K, MPa (ksi)	n	%EL, %	%RA, %	R, mm (in.)	σ _f *, MPa (ksi)	ε _f
E7-14	4.70 (0.185)	4.65 (0.183)	7.62 (0.30)	8.20 (0.32)	210.0 (30,451.0)	1194.1 (173.2)	NA NA	NA NA	NA	1736.6 (251.9)	6,180.6 (896.4)	0.2639	7.7%	1.9%	83.13 (3.273)	1758.7 (255.1)	2.0%
E7-5	4.71 (0.185)	4.69 (0.185)	7.62 (0.30)	8.20 (0.32)	210.6 (30,537.8)	1144.2 (165.9)	NA NA	NA NA	NA	1814.5 (263.2)	9,254.8 (1342.2)	0.3419	7.7%	0.9%	95.19 (3.747)	1819.2 (263.8)	0.9%
Average values					210.3 (30,494.4)	1169.1 (169.6)	NA NA	NA NA	NA	1775.6 (257.5)	7717.7 (1,119.3)	0.3029	7.7%	1.4%	89.16 3.510	1788.9 (259.5)	1.4%

* The values of true fracture strength are corrected for necking according to the Bridgman correction factor.

Table A.2: Summary of constant amplitude completely reversed fatigue test results

Specimen ID	Test control mode	Test freq., Hz	E, GPa (ksi)	At midlife ($N_{50\%}$)						$\Delta\epsilon_{p/2}^{[a]}$, %	$(2N_f)_{50\%}^{[c]}$, reversals	Failure location ^[d]
				E', GPa (ksi)	$\Delta\epsilon/2$, %	$\Delta\epsilon_p/2$ (calculated), %	$\Delta\epsilon_p/2$ (measured), %	$\Delta\sigma/2$, MPa (ksi)	σ_m , MPa (ksi)			
E7-23	strain	0.10	212.4 (30,799.1)	202.9 (29,431.8)	1.227%	0.216%	0.153%	2125.4 (308.3)	-201.4 (-29.2)	20	26	IGL(S ^[d])
E7-16	strain	0.10	209.2 (30,345.5)	200.0 (29,008.7)	1.218%	0.215%	0.163%	2108.3 (305.8)	-255.9 (-37.1)	8	16	IGL(S ^[d])
E7-8	train+load	0.10	209.2 (30,334.4)	204.3 (29,631.1)	1.096%	0.138%	0.100%	2012.6 (291.9)	-219.2 (-31.8)	40	112	IGL(S ^[d])
E7-11	train+load	0.10	208.7 (30,262.8)	202.0 (29,296.2)	1.097%	0.146%	0.093%	1998.6 (289.9)	-227.4 (-33.0)	40	92	IGL(S ^[d])
E7-1 ^[e]	train+load	0.10	213.3 (30,933.6)	217.9 (31,604.9)	0.916%	0.029%	0.058%	1866.0 (270.6)	-235.5 (-34.2)	200	296	IGL(S ^[d])
E7-12	train+load	0.10	210.1 (30,466.1)	207.0 (30,016.3)	0.902%	0.062%	0.038%	1766.1 (256.1)	-226.9 (-32.9)	200	294	IGL(S ^[d])
E7-2	train+load	0.10	205.9 (29,858.0)	205.1 (29,748.2)	0.897%	0.061%	0.033%	1758.1 (255.0)	-211.3 (-30.7)	200	306	IGL(S ^[d])
E7-7	train+load	0.50	215.6 (31,264.7)	205.7 (29,835.4)	0.697%	0.029%	0.010%	1404.3 (203.7)	-181.3 (-26.3)	400	5,008	IGL(S ^[d])
E7-15	train+load	0.50	209.8 (30,420.8)	207.2 (30,051.2)	0.698%	0.025%	0.010%	1414.3 (192.8)	-276.7 (-37.4)	400	8,590	IGL(S ^[d])
E7-21	train+load	0.50	208.8 (30,285.1)	204.3 (29,629.1)	0.694%	0.027%	0.012%	1401.0 (203.2)	-210.5 (-30.5)	400	4,836	IGL(S ^[d])
E7-6	load	2.0			0.500%			1034.3 (150.0)	0.0 (0.0)		81,236	IGL(SS ^[d])
E7-13	load	2.0			0.500%			1042.1 (151.1)	0.0 (0.0)		82,184	IGL(SS ^[d])
E7-22	load	2.0			0.500%			1034.3 (150.0)	0.0 (0.0)		63,852	IGL(SS ^[d])
E7-25	load	20.0			0.400%			827.5 (120.0)	0.0 (0.0)		189,906	IGL(SS ^[d])
E7-18	load	20.0			0.400%			827.5 (120.0)	0.0 (0.0)		1,005,066	IGL(SS ^[d])
E7-9	load	30.0			0.325%			672.2 (97.5)	0.0 (0.0)		10,000,000	No Fail
E7-17	load	30.0			0.325%			672.1 (97.5)	0.0 (0.0)		10,000,000	No Fail
E7-4	load	30.0			0.325%			672.3 (97.5)	0.0 (0.0)		10,000,000	No Fail

[a] $N_{50\%}$ is defined as the midlife cycle (for run-out tests, data is taken from the stable cycle indicated).

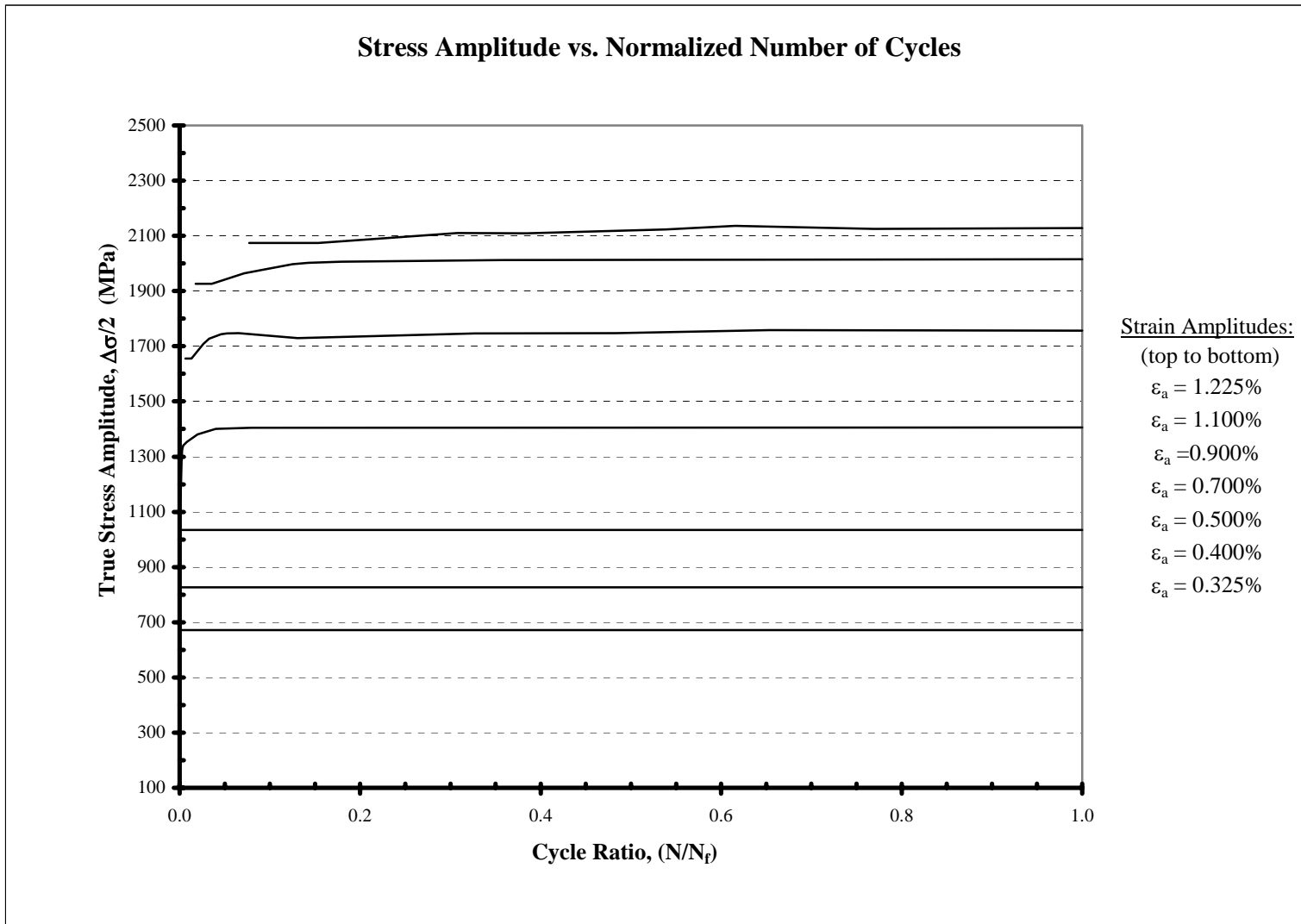


Figure A.1a: True stress amplitude versus normalized number of cycles

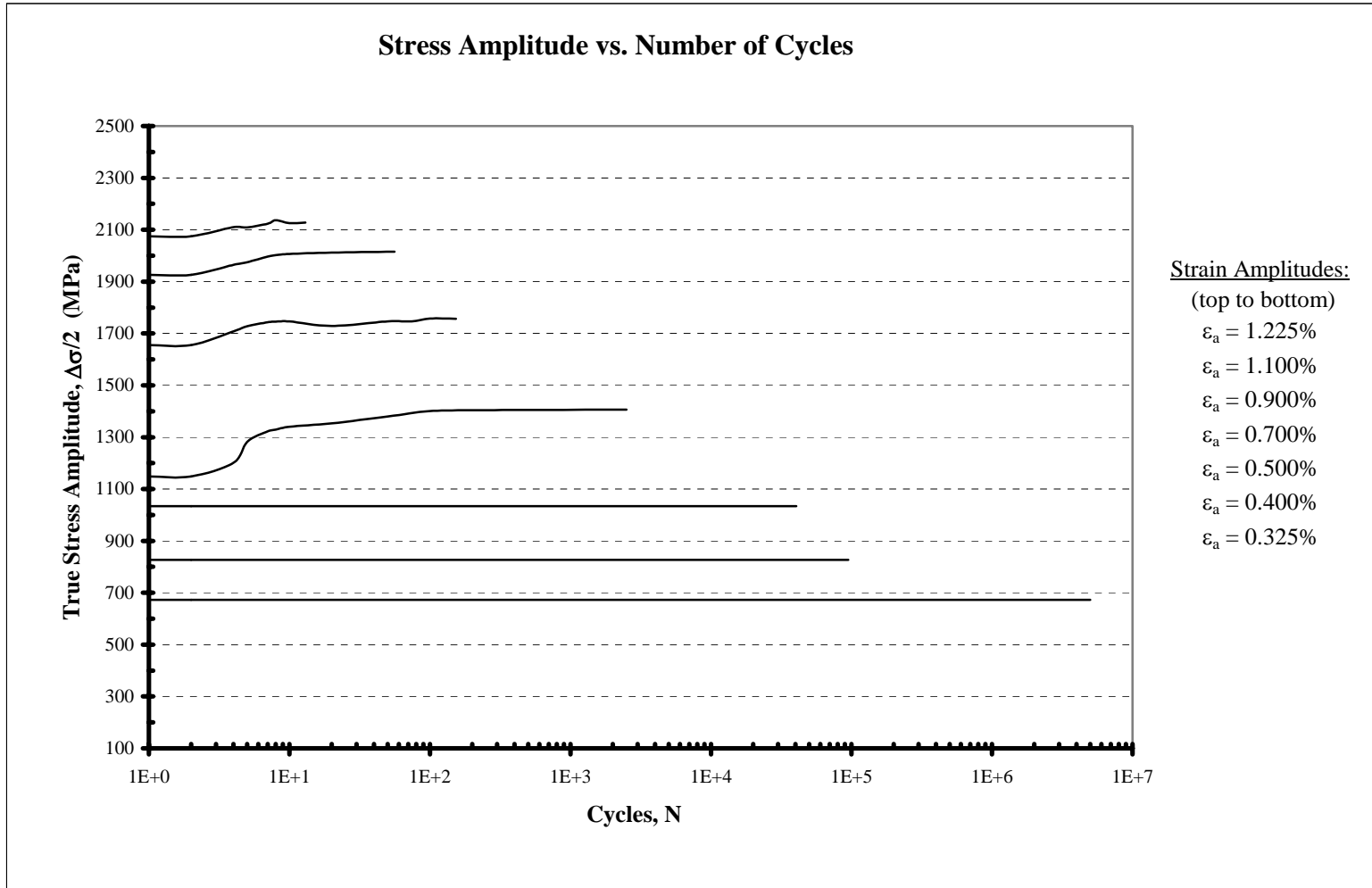


Figure A.1b: True stress amplitude versus number of cycles

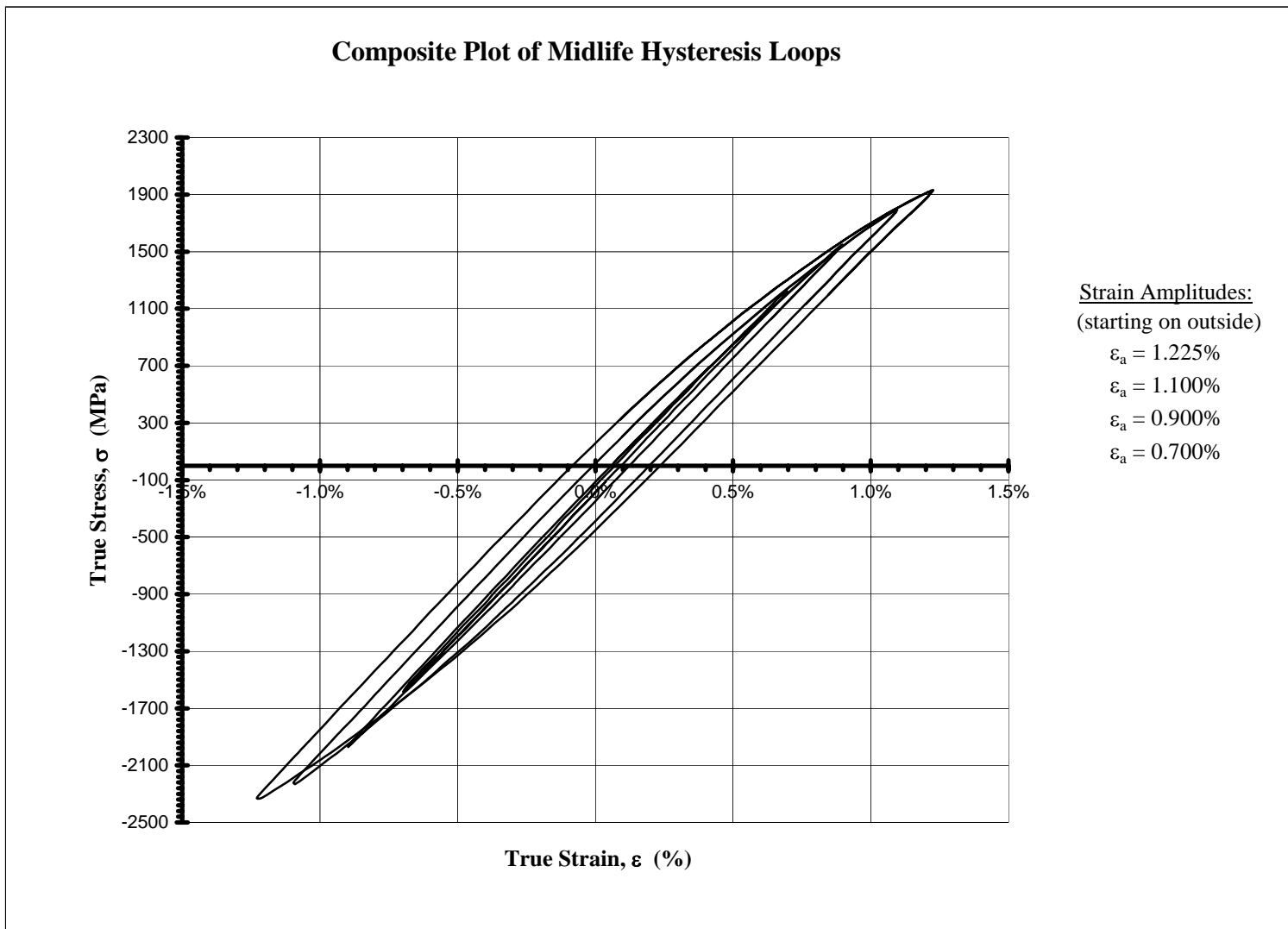


Figure A.2: Composite plot of midlife hysteresis loops